# Dynamic winding number for Floquet topological insulators with arbitrarily driving frequencies

Bo Zhu,[1] Zhi Tan,[2] Yongguan Ke,[2] and Honghua Zhong[1,*]

[1]*Institute of Mathematics and Physics, Central South University of Forestry and Technology, Changsha 410004, China*

[2]*Institute of Quantum Precision Measurement, State Key Laboratory of Radio Frequency Heterogeneous Integration, College of Physics and Optoelectronic Engineering, Shenzhen University, Shenzhen 518060, China*

(Received 2 January 2024; accepted 17 June 2024; published 26 June 2024)

Winding number and Zak phase, as topological invariants, play crucial roles in characterizing the topological phases of one-dimensional Floquet topological insulators. It is difficult to directly detect Floquet topological invariants with a unified scheme, especially for low driving frequencies. Here, by defining the dynamic winding number based on the time-averaged spin textures, we propose to use it to characterize one-dimensional Floquet topological phases with arbitrarily varying frequencies. In the high-frequency regime, both the conventional winding number and Zak phase can be fully determined by measuring the dynamic winding number of time-averaged spin textures, regardless of initial states and initial phases. In the low-frequency regime, only conventional winding number can accurately describe the system's topological phase due to the presence of large topological numbers, the Zak phase only captures the parity of the winding number and fails to characterize the number of topological edge states. However, one can still correctly characterize the Floquet topological phases through our dynamic winding number approach, in which stroboscopic measurement of spin textures is needed and the initial phases should guarantee chiral symmetry of the time-evolution operator. Our paper not only clarifies the necessity of stroboscopic measurements, but also provides a general dynamic approach for the detection of Floquet topological insulators.

DOI: 10.1103/PhysRevB.109.224315

## I. INTRODUCTION

Floquet topological insulators and their characterization have attracted a great deal of attention in both theories [1–20] and experiments [21–29]. A key concept is topological invariants, which characterize the global topological properties of Bloch wavefunctions and respond to robust topological edge states [30–35]. Unlike static systems, robust edge modes may exist in two-dimensional periodically driven systems while the Chern number of all bands are zero, which is dubbed anomalous Floquet topological phases [14–17,26,27,29]. These Floquet topological phases can be fully characterized by winding numbers [14], topological singularities of phase bands [15] defined in the momentum-time space, or $(d-1)$-dimensional band inversion surfaces [17,29]. Floquet engineering also provides a powerful approach to generate nonequilibrium topological phases with larger topological invariants, which are hard to achieve in static systems [18,20].

It is well known that both the winding number and the Zak phase can be used to characterize topological phases in one-dimensional periodic driven systems [36,37]. When the system satisfies chiral symmetry, the Zak phase is limited to the values of 0 or $\pi$, while the winding number can take any integer value. Hence, the number of edge states is directly related to the winding number rather than to the binary Zak phase. In the low-frequency regions, obtaining the Zak phase and winding number usually further requires time-domain information beyond the Floquet bands, which makes it difficult to directly detect Floquet topological invariants with arbitrarily driving frequencies. Since dynamic methods have been successfully used to characterize bulk topologies of static systems, such as long-time average of chiral position [38–40], band inversion surfaces [41–45], linked number [46,47], and dynamic winding number (DWN) [48], generalizing these dynamic methods to periodically modulated systems could potentially open a new avenue to detect Floquet topological invariants. Motivated by dynamic methods, the Floquet topological invariant can be extracted by emergent topological patterns in the momentum subspace called band inversion surfaces [17,29]. Non-Hermitian Floquet topological phases in one dimension can also be extracted via dynamic winding number defined with the time average of spin textures [49]. In particular, the method of dynamic winding number does not require any prior knowledge of topologies before and after quenched dynamics. Due to the significant differences between non-Hermitian and Hermitian systems, it is unclear how to apply the method of dynamic winding number to periodically driven Hermitian systems with arbitrarily driving frequencies.

In this paper, we consider a one-dimensional periodically driven two-band Hermitian model with chiral symmetry, which supports nontrivial Floquet topological invariants described by the conventional winding number (CWN) or Zak phase. In the high-frequency regime, we have found that the CWN and Zak phase are one-to-one correspondence, which can be measured through the DWN. Similar to the static system, the definition of DWN is based on time-averaged spin textures that are robust against various initial states and phases, and stroboscopic measurements of spin textures are

*Contact author: hhzhong115@163.com

 

not needed. In the low-frequency regime, CWN could take larger value as 2, which corresponds to 0 Zak phase due to the modulus of $2\pi$. In this case, only CWN can faithfully characterize the topological phases and correctly give the number of pairs of topological edge states. Unlike the high-frequency regime, we found that the symmetry of the effective Hamiltonian related to the evolution operator is sensitive to the initial phase of modulation. Therefore, to ensure that the evolution operator satisfies chiral symmetry, it is necessary not only to choose the appropriate initial phase but also to perform stroboscopic measurements of spin textures. According to the bulk-edge correspondence, the DWN can accurately predict the number of topologically protected Floquet edge states with arbitrarily driving frequencies. Compared with Refs. [17,49], our paper clarifies the necessity of implementing stroboscopic measurements in Floquet topological insulators and provides a unified definition of DWN for arbitrary driving frequencies. Compared to the scheme of quenched dynamics, our method to extract Floquet topological invariants is robust to various initial states, without the need to know the topologies before and after quenched dynamics.

The paper is organized as follows. In Sec. II, we introduce our physical model and give the definition of topological invariants in one-dimensional periodically driven systems. In Sec. III, we give the definition of DWN with arbitrarily driving frequencies, and the relationship between CWN, Zak phase and DWN. We focus on whether DWN can be used to simultaneously extract topological invariants CWN and Zak phase with arbitrarily driving frequencies, as well as the necessity of stroboscopic measurement. In Sec. IV, we give a brief conclusion and discussion.

## II. THE DEFINITION OF TOPOLOGICAL INVARIANTS WITH ARBITRARY DRIVING FREQUENCIES

We start by considering one-dimensional periodically driven two-band model. The Hamiltonian in the momentum space is composed of the Pauli matrices

$$H(k,t) = h_i(k,t)\sigma_i + h_j(k,t)\sigma_j. \tag{1}$$

Here, $i \neq j$ and $i, j \in (x, y, z)$, $k$ is the quasimomentum, $h_{i(j)}(k,t)$ are periodic functions of $k$ and $t$. Thus, the Hamiltonian with quasimomentum and time translation invariance $H(k,t) = H(k+2\pi,t) = H(k,t+T)$, $T = 2\pi/\omega$ is the period of time and $\omega$ corresponds to the driving frequency. According to the Floquet theorem [50,51], the Floquet-Bloch ansatz can be given by $|\psi_{k,\mu}(t)\rangle = e^{-i\epsilon_{k,\mu}t}|\varphi_{k,\mu}(t)\rangle$, where $|\varphi_{k,\mu}(t)\rangle$ is the Floquet states, $\epsilon_{k,\mu}$ is the quasienergy of the Floquet state, and $\mu = \pm$ expresses the band index. The Floquet states $|\varphi_{k,\mu}(t)\rangle$ satisfy the eigenvalue equation

$$\begin{aligned} \widetilde{H}(k,t)|\varphi_{k,\mu}(t)\rangle &= \epsilon_{k,\mu}|\varphi_{k,\mu}(t)\rangle, \\ \widetilde{H}(k,t) &= H(k,t) - i\partial_t, \end{aligned} \tag{2}$$

where $\widetilde{H}(k,t)$ is the Floquet operator. Due to the periodicity of time, the Floquet states $|\varphi_{k,\mu}(t)\rangle$ can be expressed in terms of their Fourier components $|\varphi_{k,\mu,\chi}\rangle$,

$$|\varphi_{k,\mu}(t)\rangle = \sum_{\chi=-\infty}^{\infty} e^{-i\chi\omega t}|\varphi_{k,\mu,\chi}\rangle, \tag{3}$$

where $|\varphi_{k,\mu,\chi}\rangle$ is the $\chi$th Floquet state of the $\mu$ band. Then one can obtain the quasienergies $\epsilon_{k,\mu,\chi}$ and the corresponding Floquet states $|\varphi_{k,\mu,\chi}\rangle$ by diagonalizing the matrix

$$\begin{aligned} \langle\langle\varphi_{k,\mu',\chi'}|\widetilde{H}(k,t)|\varphi_{k,\mu,\chi}\rangle\rangle &= S^{\mu,\mu'}_{\chi,\chi'}(k) + \chi\omega\delta_{\chi,\chi'}\delta_{\mu,\mu'}, \\ S^{\mu,\mu'}_{\chi,\chi'}(k) &= \frac{1}{T}\int_0^T s^{\mu,\mu'}(k,t)e^{-i(\chi-\chi')\omega t}dt, \end{aligned} \tag{4}$$

where $s^{\mu,\mu'}(k,t)$ is the matrix element of the Hamiltonian $H(k,t)$, $\chi\omega\delta_{\chi,\chi'}$ is the Fourier space representation of $-i\partial_t$, and $\langle\langle\cdots\rangle\rangle = \int_0^T\langle\cdots\rangle dt/T$ is the composed scalar product, which gets rid of the time dependence [51]. Generally, for such a periodically driven system, topological invariants can be defined by the Floquet states.

### A. Conventional winding number (CWN)

We know that the definition of winding number requires the systems to satisfy chiral symmetry. In order to provide a definition of CWN for arbitrary driving frequencies, it is particularly important to determine the chiral symmetry operators for the Floquet systems. In this section, we will give the chiral symmetry operators corresponding to the effective static Hamiltonian in both high-frequency and low-frequency regions, as well as the corresponding definition of CWN.

Because different Floquet blocks mutually couple, we need to numerically solve Eq. (4). Numerically, one can obtain an effective Hamiltonian by reasonably truncating the Floquet space. If we consider the truncation number $Y = 2n+1$, the effective Hamiltonian $H^{\text{eff}}$ can be given by the $2Y\times 2Y$ matrix, via selecting the Floquet blocks ranging from $\chi \in [-n, n]$,

$$H^{\text{eff}}(k) = \begin{pmatrix} \ddots & \vdots & \vdots & \vdots & \iddots \\ \cdots & H^{\text{eff}}_{-1,-1} & H^{\text{eff}}_{-1,0} & H^{\text{eff}}_{-1,1} & \cdots \\ \cdots & H^{\text{eff}}_{0,-1} & H^{\text{eff}}_{0,0} & H^{\text{eff}}_{0,1} & \cdots \\ \cdots & H^{\text{eff}}_{1,-1} & H^{\text{eff}}_{1,0} & H^{\text{eff}}_{1,1} & \cdots \\ \iddots & \vdots & \vdots & \vdots & \ddots \end{pmatrix}, \tag{5}$$

with

$$\begin{aligned} H^{\text{eff}}_{\chi,\chi'}(k) &= S^{\mu,\mu'}_{\chi,\chi'}(k) + \chi\omega\delta_{\chi,\chi'}\delta_{\mu,\mu'}, \\ S^{\mu,\mu'}_{\chi,\chi'}(k) &= \frac{1}{T}\int_0^T s^{\mu,\mu'}(k,t)e^{-i(\chi-\chi')\omega t}dt \\ &= \begin{pmatrix} 0 & \rho_{\chi,\chi'} \\ \rho^*_{\chi,\chi'} & 0 \end{pmatrix}. \end{aligned} \tag{6}$$

Here $\rho_{\chi,\chi'}$ and $\rho^*_{\chi,\chi'}$ are a matrix element of $S^{\mu,\mu'}_{\chi,\chi'}$.

To discuss the symmetry of the effective Hamiltonian (5), we define an exchange operator $\Upsilon$, which satisfies $\Upsilon G = G'$, where $G = [\cdots, A_{-1}, B_{-1}, A_0, B_0, A_1, B_1, \cdots]^T$ and $G' = [\cdots, A_{-1}, A_0, A_1, \cdots, B_{-1}, B_0, B_1, \cdots]^T$. In the basis

of the exchange operator, $\Upsilon$ must be diagonalized through the unitary matrix $U_1$, which satisfies $U_1\Upsilon U_1^{-1} = \mathrm{diag}[\mathrm{eig}(\Upsilon)]$. Transforming Hamiltonian (5) by using the unitary matrix $U_1$, we can obtain

$$\tilde{H}^{\mathrm{eff}} = U_1 H^{\mathrm{eff}} U_1^{-1} = \begin{pmatrix} R & K \\ K^{\dagger} & R \end{pmatrix}, \tag{7}$$

with

$$K = \begin{pmatrix} \ddots & \vdots & \vdots & \vdots & \iddots \\ \cdots & \rho_{-1,-1} & \rho_{-1,0} & \rho_{-1,1} & \cdots \\ \cdots & \rho_{0,-1} & \rho_{0,0} & \rho_{0,1} & \cdots \\ \cdots & \rho_{1,-1} & \rho_{1,0} & \rho_{1,1} & \cdots \\ \iddots & \vdots & \vdots & \vdots & \ddots \end{pmatrix},$$

and

$$R = \begin{pmatrix} \ddots & & & & & & \\ & 2\omega & & & & & \\ & & \omega & & & & \\ & & & 0 & & & \\ & & & & -\omega & & \\ & & & & & -2\omega & \\ & & & & & & \ddots \end{pmatrix}.$$

In this way the Hamiltonian $\tilde{H}^{\mathrm{eff}}$ also can satisfy chiral symmetry $\Lambda\tilde{H}^{\mathrm{eff}}\Lambda^{-1} = -\tilde{H}^{\mathrm{eff}}$, where the chiral symmetry operator is $\Lambda = \sigma_z \bigotimes \Theta$, with $Y \times Y$ matrix

$$\Theta = \begin{pmatrix} & & & & & & \iddots \\ & & & & & 1 & \\ & & & & -1 & & \\ & & & 1 & & & \\ & & -1 & & & & \\ & 1 & & & & & \\ \iddots & & & & & & \end{pmatrix}$$

for the case of matrix element $\rho_{\chi,\chi'} = (-1)^{\chi-\chi'}\rho_{-\chi,-\chi'}$, and

$$\Theta = \begin{pmatrix} & & & & & & \iddots \\ & & & & & 1 & \\ & & & & 1 & & \\ & & & 1 & & & \\ & & 1 & & & & \\ & 1 & & & & & \\ \iddots & & & & & & \end{pmatrix}$$

for the case of matrix element $\rho_{\chi,\chi'} = \rho_{-\chi,-\chi'}$. The Hamiltonian (7) can be transformed into a block off-diagonal form in the basis of chiral symmetric operators, where the chiral symmetry operator $\Lambda$ needs to be diagonalized by the unitary matrix $U_2$, which satisfies $U_2\Lambda U_2^{-1} = \mathrm{diag}[\mathrm{eig}(\Lambda)]$. Transforming Hamiltonian (7) by using the unitary matrix $U_2$, we can obtain

$$U_2\tilde{H}^{\mathrm{eff}}U_2^{-1} = \begin{pmatrix} 0 & F(k) \\ F^{\dagger}(k) & 0 \end{pmatrix}. \tag{8}$$

Then the definition of CWN in the low-frequency regime can be given by

$$\begin{aligned} w_{\pm} &= \frac{1}{2\pi i}\oint_S \partial_k Ln\{\mathrm{Det}[F(k)]\}dk \\ &= \frac{1}{2\pi}\oint_S \partial_k \phi_{ij} dk, \end{aligned} \tag{9}$$

where $S$ is a closed loop with $k$ varying from 0 to $2\pi$, and $\phi_{ij} = \arctan\left(\frac{\mathrm{Im}\{\mathrm{Det}[F(k)]\}}{\mathrm{Re}\{\mathrm{Det}[F(k)]\}}\right)$ is the equilibrium azimuthal angle.

### B. CWN in the high-frequency regime

In the high-frequency regime, the second term in the right-hand side of Eq. (4) dominates, and the couplings between nearest-neighboring Floquet blocks can be viewed as a perturbation. Thus one can obtain an effective static Hamiltonian $H^{\mathrm{eff}}$ given by the $2\times2$ matrix via selecting the Floquet Block $\chi = \chi' = 0$,

$$\begin{aligned} H^{\mathrm{eff}}(k) &= \begin{pmatrix} S_{0,0}^{+,+}(k) & S_{0,0}^{+,-}(k) \\ S_{0,0}^{-,+}(k) & S_{0,0}^{-,-}(k) \end{pmatrix} \\ &= h_i^{\mathrm{eff}}(k)\sigma_i + h_j^{\mathrm{eff}}(k)\sigma_j. \end{aligned} \tag{10}$$

The corresponding quasienergy can be given by

$$\epsilon_{\mu}(k) = \mu\sqrt{\left[h_i^{\mathrm{eff}}(k)\right]^2 + \left[h_j^{\mathrm{eff}}(k)\right]^2}.$$

The characterization of topological property of the system can be given by Eq. (10). It is worth noting that the effective Hamiltonian (10) has chiral symmetry $\Lambda H^{\mathrm{eff}}(k)\Lambda = -H^{\mathrm{eff}}(k)$ with $\Lambda = i\sigma_i\sigma_j$. The CWN for different Floquet bands are the same, which can be denote as

$$w_{\pm} = \frac{1}{2\pi}\oint_S dk \frac{h_j^{\mathrm{eff}}\partial_k h_i^{\mathrm{eff}} - h_i^{\mathrm{eff}}\partial_k h_j^{\mathrm{eff}}}{{\epsilon_{\mu}}^2}, \tag{11}$$

where $S$ is a closed loop with $k$ varying from 0 to $2\pi$. If we define an equilibrium azimuthal angle $\phi_{ij}(k) = \arctan(h_i^{\mathrm{eff}}/h_j^{\mathrm{eff}})$, Eq. (11) can be written as

$$\begin{aligned} w_{\pm} &= \frac{1}{2\pi}\oint_S dk \frac{h_j^{\mathrm{eff}}\partial_k h_i^{\mathrm{eff}} - h_i^{\mathrm{eff}}\partial_k h_j^{\mathrm{eff}}}{{\epsilon_{\mu}}^2} \\ &= \frac{1}{2\pi}\oint_S dk \frac{h_j^{\mathrm{eff}}\partial_k h_i^{\mathrm{eff}} - h_i^{\mathrm{eff}}\partial_k h_j^{\mathrm{eff}}}{\left(h_i^{\mathrm{eff}}\right)^2 + \left(h_j^{\mathrm{eff}}\right)^2} \\ &= \frac{1}{2\pi}\oint_S \partial_k \phi_{ij} dk. \end{aligned} \tag{12}$$

### C. Zak phase

The Zak phase $\Gamma$ is closely related to the winding number by $w_{\pm}\pi \bmod 2\pi$ in the $z$-class insulators [52,53]. The Zak phase, limited to 0 and $\pi$ due to modulo operation, usually can predict the existence (with the relevant cumulative phase being $\pi$) or absence (vanishing cumulative phase) of topological zero-energy edge states in specific gaps. However, for nontrivial even winding number supporting topological edge states, the Zak phase is equal to 0, which cannot predict the existence of topological edge states. For our periodically driven systems with arbitrary driving frequencies, it is unclear when the Zak phase can faithfully characterize the topological

properties and when the Zak phase fails. To compute the Zak phase of the Floquet quasienergy spectrum, one usually needs to truncate the Floquet space [36,37]. All numbers of replicas of quasienergies need to be chosen, and then all relevant transitions at the desired energy are kept. The Zak phase for a specific gap is given by summing up $\Gamma^{(\mu,\chi)}$ for all bands below the gap, where $\Gamma^{(\mu,\chi)} = i\oint_k \langle\varphi_{k,\mu,\chi}|\partial_k|\varphi_{k,\mu,\chi}\rangle dk$. If we consider the truncation number $Y = 2n+1$ (corresponding to $\chi \in [-n, n]$), $2Y$ Floquet quasienergy bands are obtained. For simplicity, we mark $\Gamma^{(\mu,\chi)}$ as $\Gamma^{(l)}$, and $|\varphi_{k,\mu,\chi}\rangle$ as $|\varphi_{k,l}\rangle$, where $l$ is the band index. For a gap between the $Y$th and $(Y+1)$th bands (corresponding to the zero-energy gap), the Zak phase $\Gamma$ can be defined as

$$\Gamma = \sum_{l=1}^{Y} \Gamma^{(l)} = \sum_{l=1}^{Y} \left[ i \oint_k \langle\varphi_{k,l}|\partial_k|\varphi_{k,l}\rangle dk \right]. \tag{13}$$

It should be noted that a reasonable selection of truncation numbers $Y$ is usually associated with the driving frequency. For example, one can select the truncation number $Y = 1$ in the high-frequency regime and $Y = 100$ in the low-frequency regime.

## III. EXTRACTING TOPOLOGICAL INVARIANTS USING DWN FOR ARBITRARILY DRIVING FREQUENCIES

In this section, we will introduce a unified dynamic approach for measuring topological invariants in both high-frequency and low-frequency regimes. We first provide the definition of DWN with arbitrarily driving frequencies, and then discuss how to extract topological invariants by utilizing the DWN, including the CWN and Zak phase.

### A. High-frequency regime ($\omega \gg t_{1,2}$)

In the high-frequency regime, we consider an arbitrary initial state $|\Psi_k(0)\rangle = \sum_\mu c_{k,\mu}|\varphi_{k,\mu}\rangle$, and then the time evolution of $|\Psi_k(t)\rangle$ satisfies

$$|\Psi_k(t)\rangle = \sum_\mu c_{k,\mu} e^{-i\epsilon_{k,\mu}t}|\varphi_{k,\mu}\rangle, \tag{14}$$

with $c_{k,\mu} = \langle\varphi_{k,\mu}|\Psi_k(0)\rangle$. According to the time evolution of the state, the spin textures are given by the expectation values of the Pauli matrices, $\langle\Psi_k(t)|\sigma_{i(j)}|\Psi_k(t)\rangle$. It is worth noting that the expected value of the Pauli matrix is an observable quantity in the experiment, which is related to the spin population $N_{\uparrow(\downarrow)}(k)$. The spin population $N_{\uparrow(\downarrow)}(k)$ with different momentums can be measured in the experiment by spin-resolved time-of-flight absorption imaging [41]. Thus the expected value of the Pauli matrix $\sigma_z$ can be given via the spin population difference, $\langle\Psi_k(t)|\sigma_z|\Psi_k(t)\rangle = (N_\uparrow(k) - N_\uparrow(k))/(N_\uparrow(k) + N_\uparrow(k))$. Similarly, the spin polarization $\langle\Psi_k(t)|\sigma_{x(y)}|\Psi_k(t)\rangle$ also can be transferred to the spin population difference by applying $\pi/2$ pulse, that is, $\langle\Psi_k(t)|\sigma_{x(y)}|\Psi_k(t)\rangle = \langle\Psi_k(t)|e^{-i\frac{\pi}{2}\frac{\sigma_{y(x)}}{2}}\sigma_z e^{i\frac{\pi}{2}\frac{\sigma_{y(x)}}{2}}|\Psi_k(t)\rangle$. Then, according to the method in Ref. [48], one can obtain the long-time averages

$$\overline{\sigma_{i(j)}} = \lim_{t'\to\infty}\frac{1}{t'}\int_0^{t'}\langle\Psi_k(t)|\sigma_{i(j)}|\Psi_k(t)\rangle dt, \tag{15}$$

and the DWN in high-frequency regime can be defined as

$$w_d = \frac{1}{2\pi}\oint_S \partial_k \eta_{ij}(k) dk, \tag{16}$$

where $S$ is a closed loop in the parameter space $k$, and $\eta_{ij}(k) = \arctan(\overline{\sigma_i}/\overline{\sigma_j})$ is the dynamical azimuthal angle. Despite the fact that the dynamical azimuthal angle depends on the initial state, it is convergent in the long time. The long-time average of $\langle\Psi_k(t)|\sigma_i|\Psi_k(t)\rangle$ is given by

$$\begin{aligned}\overline{\sigma_i} &= \lim_{t'\to\infty}\frac{1}{t'}\int_0^{t'}\langle\Psi_k(t)|\sigma_i|\Psi_k(t)\rangle dt \\ &= \lim_{t'\to\infty}\frac{1}{t'}\int_0^{t'}\sum_{\mu,\mu'} c_{k,\mu}c^*_{k,\mu'}e^{-i(\epsilon_\mu - \epsilon^*_{\mu'})t}\langle\varphi_{k,\mu'}|\sigma_i|\varphi_{k,\mu}\rangle dt.\end{aligned} \tag{17}$$

For the Hermitian systems with chiral symmetry, the energies are purely real and $\epsilon_{k,\pm} = -\epsilon_{k,\mp}$. Thus, Eq. (17) can be simplified as

$$\begin{aligned}\overline{\sigma_i} &\cong \sum_\mu |c_{k,\mu}|^2\langle\varphi_{k,\mu}|\sigma_i|\varphi_{k,\mu}\rangle \\ &= (|c_{k,+}|^2 - |c_{k,-}|^2)\frac{h_i^{\text{eff}}}{\epsilon_{k,+}}.\end{aligned} \tag{18}$$

Here, to avoid missing the information from $h_i^{\text{eff}}$, we require $|c_{k,+}|^2 \neq |c_{k,-}|^2$. Combining the definitions of $\phi_{ij}(k)$ and $\eta_{ij}(k)$, we can immediately conclude that the CWN is equal to the DWN in the high-frequency regime,

$$w_\pm = w_d. \tag{19}$$

To verify our theory, as an example, we consider a dimer chain coupled to an ac electric field, with hoppings $t_1$ and $t_2$, and periodic boundary conditions. The ac electric field $E(t) = -\partial_t F(t)$ is given by the vector potential $F(t) = \xi\sin(\omega t + \theta)$, where $\xi$ is the driving amplitude, and $\theta$ is the initial phase. By means of the minimal coupling [51], one can arrive at the time-dependent Hamiltonian

$$H(k,t) = \begin{pmatrix} 0 & \aleph \\ \aleph^* & 0 \end{pmatrix} = h_x(k,t)\sigma_x + h_y(k,t)\sigma_y, \tag{20}$$

with

$$\begin{aligned}\aleph &= t_1 e^{-i(k+F(t))b_0} + t_2 e^{i(k+F(t))(a_0-b_0)}, \\ h_x(k,t) &= t_1\cos[(k+F(t))b_0] + t_2\cos[(k+F(t))(a_0-b_0)], \\ h_y(k,t) &= t_1\sin[(k+F(t))b_0] - t_2\sin[(k+F(t))(a_0-b_0)],\end{aligned}$$

where $a_0$ is the lattice translation vector, and $b_0$ is the intradimer distance. For simplicity, we only consider $a_0 = 1$ and $b_0 = 0$, corresponding to the situation that the one-dimensional chain forms zigzag, and the electric field is in perpendicular to the $t_1$ bonds. In the high-frequency regime, an effective static Hamiltonian can be obtained based on previous analysis

$$H^{\text{eff}}(k) = h_x^{\text{eff}}(k)\sigma_x + h_y^{\text{eff}}(k)\sigma_y. \tag{21}$$

Here, $h_x^{\text{eff}}(k) = t_1 + t_2\cos(k)J_0(\xi)$, $h_y^{\text{eff}}(k) = -t_2\sin(k)J_0(\xi)$, and $J_0(\xi)$ is the zero-order Bessel function. Note that the effective Hamiltonian remains invariant in the high-frequency

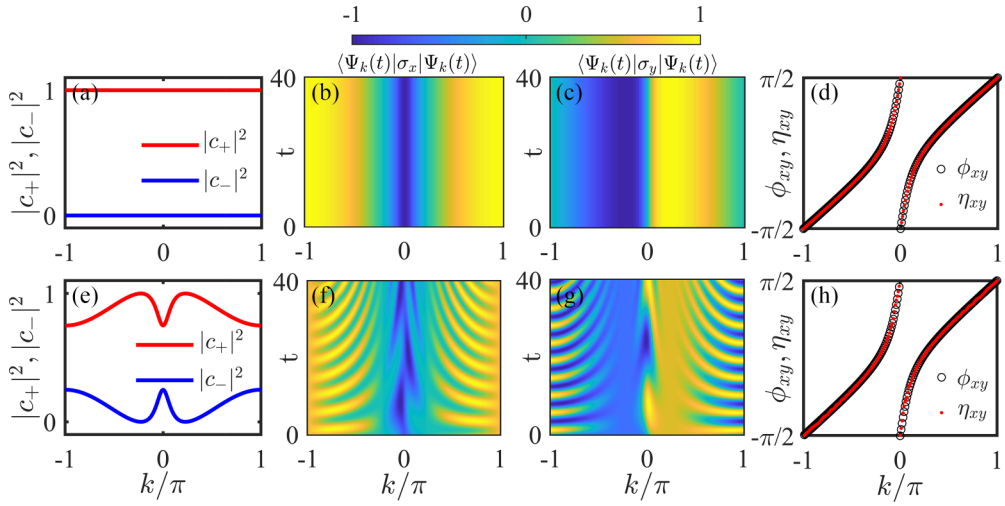


FIG. 1. Extracting conventional winding number via dynamic winding number. (Top row) (a) We consider the eigenstates of the system as the initial states satisfying $|c_+|^2 = 1$ and $|c_-|^2 = 0$. (b) and (c) respectively correspond to the time evolution of the spin textures $\langle\Psi_k(t)|\sigma_x|\Psi_k(t)\rangle$ and $\langle\Psi_k(t)|\sigma_y|\Psi_k(t)\rangle$, and (d) the equilibrium azimuthal angle $\phi_{xy}$ and dynamical azimuthal angle $\eta_{xy}$ as functions of $k$. (Bottom row) (e) We consider a random initial state satisfying $|c_+|^2 \neq |c_-|^2$. (f) and (g) respectively correspond to time evolution of the spin textures $\langle\Psi_k(t)|\sigma_x|\Psi_k(t)\rangle$ and $\langle\Psi_k(t)|\sigma_y|\Psi_k(t)\rangle$, and (h) the equilibrium azimuthal angle $\phi_{xy}$ and dynamical azimuthal angle $\eta_{xy}$ as functions of $k$. The other parameters are chosen as $t_1 = 0.3, t_2 = 1, \xi = 4$, and $\omega = 10$.

regime, regardless of the initial phase $\theta$. To clarify that the initial state has little influence on the dynamical azimuthal angle, we calculate the time evolution of spin textures $\langle\Psi_k(t)|\sigma_{x(y)}|\Psi_k(t)\rangle$ based on different initial states. We further obtain the dynamical azimuthal angle $\eta_{xy}$ by taking their long-time averages, as shown in Figs. 1(a)–1(h). As an example, we select $t_1 = 0.3, t_2 = 1$, and $\xi = 4$, which corresponds to the nontrivial topological phase with CWN $w_\pm = 1$. In Fig. 1(a), we first consider the eigenstates of the system as the initial states, satisfying $|c_+|^2 = 1$ and $|c_-|^2 = 0$. Figures 1(b) and 1(c) respectively correspond to the time evolution of the spin textures $\langle\Psi_k(t)|\sigma_x|\Psi_k(t)\rangle$ and $\langle\Psi_k(t)|\sigma_y|\Psi_k(t)\rangle$. According to the effective static Hamiltonian and the long-time averages of spin textures, Fig. 1(d) shows the equilibrium azimuthal angle $\phi_{xy}$ and the dynamical azimuthal angle $\eta_{xy}$ as functions of $k$, respectively. Obviously, the spin textures remain unchanged over time $t$, and the dynamical azimuthal angle $\eta_{xy}$ perfectly matches the equilibrium azimuthal angle $\phi_{xy}$. Then the DWN can be obtained via the integral of a piecewise function

$$w_d = \frac{1}{2\pi}\left(\int_{-\pi}^{k_c} \partial_k \eta_{xy} dk + \int_{k_c}^{\pi} \partial_k \eta_{xy} dk\right), \tag{22}$$

where $k_c = 0$ represents the point of discontinuity in the variation of $\eta_{xy}$ with respect to parameter $k$. Obviously, the DWN is equal to 1, which is the same as the CWN. From the above result, we can see that when one selects the eigenstate of the system as the initial state, $\overline{\sigma_{x(y)}}$ can be replaced with $\langle\Psi_k(t)|\sigma_{x(y)}|\Psi_k(t)\rangle$ at any given time. This substitution facilitates the extraction of the dynamical azimuthal angle in the experiment. However, accurately preparing the eigenstate of the system as an initial state in the experiment is a challenge. Therefore, we will discuss the impact of a random initial state on the measurement result, as shown in Figs. 1(e) and 1(f). In detail, we give the projection of the random initial state on the eigenstate of the system, which satisfies a relatively loose condition $|c_{k,+}|^2 \neq |c_{k,-}|^2$, see Fig. 1(e). Similarly, we give the time evolution of spin textures $\langle\Psi_k(t)|\sigma_{x(y)}|\Psi_k(t)\rangle$ and $\langle\Psi_k(t)|\sigma_{x(y)}|\Psi_k(t)\rangle$ in Figs. 1(f) and 1(g), respectively. Although the spin textures oscillate with a momentum-dependent period $\tilde{T}_k = \pi/|\epsilon_{k,\mu}|$, the dynamical azimuthal angle still remains consistent with the equilibrium azimuthal angle. Thus, we can also obtain the DWN $w_d = w_\pm = 1$. The above results demonstrate that it is feasible to extract the CWN by using DWN in the high-frequency regime, which is consistent with our theoretical prediction.

As a comparison, we also give the $\Gamma/\pi$, CWN and DWN as a function of the driving amplitude $\xi$ in the high-frequency regime, see Fig. 2(a). To verify the bulk-edge correspondence, we also give the quasienergy spectra of the Hamiltonian (20) under open boundary condition, as shown in Fig. 2(b). Obviously, the DWN is in good agreement with the CWN and Zak phase, $w_d = w_\pm = \Gamma/\pi$, and can successfully predict the topological phase transition and zero-energy modes. In Fig. 2(c), we present the topological phase diagram in the parameter plane $(\xi, t_1)$ by using the definitions of DWN, where the red solid and blue-dotted lines represent the phase boundaries determined by $\Gamma/\pi$ and $w_\pm$, respectively. The gray regions correspond to the nontrivial topological phase, which exhibits the presence of topological zero-energy modes with $w_d = w_\pm = \Gamma/\pi = 1$. The white regions correspond to the topologically trivial phase, which lacks topological zero-energy modes with $w_d = w_\pm = \Gamma/\pi = 0$. Regardless of trivial or topological regions, our dynamic approach consistently and accurately extracts the Zak phase and CWN in the high-frequency regime.

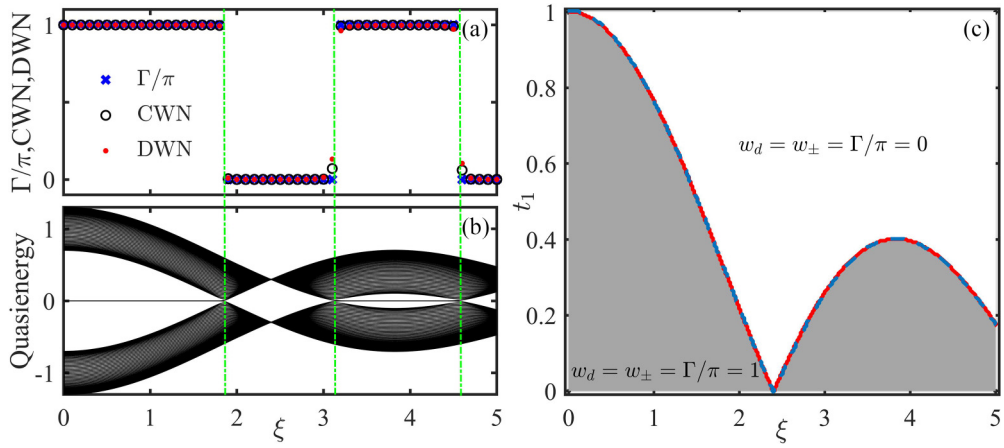


FIG. 2. (a) Topological invariant Zak phase $\Gamma/\pi$, CWN, and DWN as functions of driving amplitude $\xi$ in parameters $t_1 = 0.3$, $t_2 = 1$, and $\Omega = 10$. (b) The quasienergy spectra under open boundary condition. (c) Topological phase diagram in the parameter plane $(\xi, t_1)$, the other parameters are chosen as $t_2 = 1$ and $\omega = 10$.

### B. Low-frequency regime ($\omega \simeq t_{1,2}$)

In the low-frequency regime, depending on the symmetry of the evolution operator, the definition of the DWN needs to be modified. We also consider an initial state $|\Psi_k(0)\rangle$ that satisfies a relatively loose condition $|c_{k,+}|^2 \neq |c_{k,-}|^2$, where $c_{k,\mu} = \langle\varphi_{k,\mu}|\Psi_k(0)\rangle$. $|\varphi_{k,\mu}\rangle$ are the eigenstates of effective Hamiltonian $H_s^{\rm eff}(k)$. The time evolution of $|\Psi_k(T)\rangle$ satisfy

$$\begin{aligned}|\Psi_k(T)\rangle &= \tilde{T}\exp\left[-i\int_0^T H(k,t)dt\right]|\Psi_k(0)\rangle \\ &= U_s(k,T)|\Psi_k(0)\rangle,\end{aligned} \tag{23}$$

where $\tilde{T}$ denotes the time ordering, and $U_s(k,T)$ represents time-evolution operator from 0 to $T$. According to the evolution operator, the Floquet bands of the first Floquet Brillouin zone ($[-\pi/T, \pi/T]$) are characterized by the effective Hamiltonian $H_s^{\rm eff}(k) \equiv i\log U_s(k,T)/T$. Compared to the case of effective Hamiltonian $H^{\rm eff}$, there can exist the same energy spectrum for the first Floquet Brillouin zone and identical topology for a zero-energy gap. However, $H_s^{\rm eff}(k)$ may lose original chiral symmetry due to the existence of Floquet band couplings in the low-frequency regime. For example, the original Hamiltonian (20) clearly satisfies chiral symmetry $\sigma_z H(k,t)\sigma_z^{-1} = -H(k,t)$, where the Pauli matrix $\sigma_z$ corresponds to the chiral symmetry operator. However, if $F(t) = F(-t)$, the original chiral symmetry can be retained $\sigma_z H_s^{\rm eff}(k)\sigma_z^{-1} = -H_s^{\rm eff}(k)$, and if $F(t) \neq F(-t)$, the original chiral symmetry obviously will be broken $\sigma_z H_s^{\rm eff}(k)\sigma_z^{-1} \neq -H_s^{\rm eff}(k)$, as shown in Fig. 3. To analyze the above conclusion, we can numerically write the effective Hamiltonian $H_s^{\rm eff}(k)$ in the form of Pauli matrix,

$$\begin{aligned}H_s^{\rm eff}(k) &= h_x^{\rm eff}(k)\sigma_x + h_y^{\rm eff}(k)\sigma_y + h_z^{\rm eff}(k)\sigma_z, \\ h_x^{\rm eff}(k) &= \varepsilon_+(k)\langle u_+(k)|\sigma_x|u_+(k)\rangle, \\ h_y^{\rm eff}(k) &= \varepsilon_+(k)\langle u_+(k)|\sigma_y|u_+(k)\rangle, \\ h_z^{\rm eff}(k) &= \varepsilon_+(k)\langle u_+(k)|\sigma_z|u_+(k)\rangle,\end{aligned} \tag{24}$$

where $\varepsilon_+(k)$ and $|u_+(k)\rangle$ are the quasienergy and the corresponding eigenstate of the effective Hamiltonian $H_s^{\rm eff}(k)$, respectively. Then, if the value of $\langle u_+(k)|\sigma_z|u_+(k)\rangle$ is zero for all quasimomentum $k$, it means that the effective Hamiltonian $H_s^{\rm eff}(k)$ will retain the original chiral symmetry, otherwise, the original chiral symmetry is broken. In Fig. 3, we give the value of $\langle u_+(k)|\sigma_z|u_+(k)\rangle$ as a function of quasimomentum $k$ for different initial phases $\theta$ and driving frequencies $\omega$. When we choose the initial phases $\theta = \frac{\pi}{2}, \frac{3\pi}{2}$ [corresponding to $F(t) = F(-t)$], the values of $\langle u_+(k)|\sigma_z|u_+(k)\rangle$ are zero for all quasimomentum $k$, regardless of the changes of driving frequencies $\omega$, see the blue and carmine lines in Figs. 3(a)–3(d). However, when we choose the initial phases $\theta = 0, \frac{\pi}{3}, \pi$ [corresponding to $F(t) \neq F(-t)$], the values of $\langle u_+(k)|\sigma_z|u_+(k)\rangle$ are sensitive to the changes of quasi-momentum $k$, and this dependence becomes weak with the increase of driving frequency $\omega$, see the black, red and green lines in Figs. 3(a)–3(d). If the driving frequency is sufficiently high, the system will always retain its original chiral symmetry regardless of the changes of the initial phases, see Fig. 3(d).

To ensure that DWN accurately represents the topological properties of the original driving system, it is necessary to restore the original chiral symmetry of $H_s^{\rm eff}(k)$ through certain constraints. Based on the above discussion, we propose

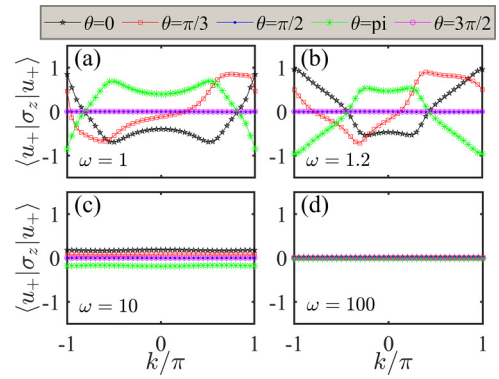


FIG. 3. The value of $\langle u_+(k)|\sigma_z|u_+(k)\rangle$ as a function of quasimomentum $k$ for different initial phases and driving frequencies. The other parameters are chosen as $t_1 = 0.3$, $t_2 = 1$, and $\xi = 1$.

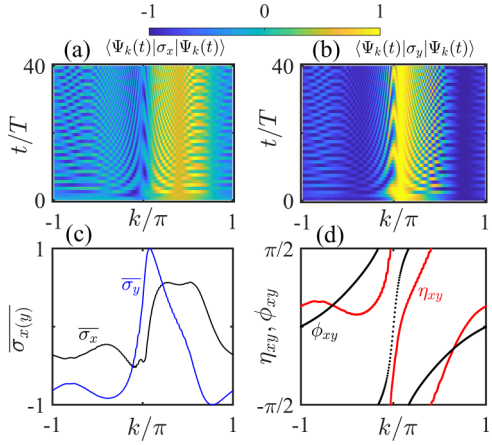


FIG. 4. Extracting conventional winding number via dynamic winding number. (a) and (b) respectively show the time evolution of the stroboscopic spin textures $\langle\psi(k,t)|\sigma_x|\psi(k,t)\rangle$ and $\langle\psi(k,t)|\sigma_y|\psi(k,t)\rangle$. (c) Long-time average of stroboscopic spin textures $\overline{\sigma_x}$ (black line) and $\overline{\sigma_y}$ (blue line) as a function of $k$, and (d) the equilibrium azimuthal angle $\phi_{xy}$ and dynamical azimuthal angle $\eta_{xy}$ as functions of $k$. The other parameters are chosen as $t_1$=0.3, $t_2$=1, $\xi = 4$, and drive frequency $\omega = 1.2$.

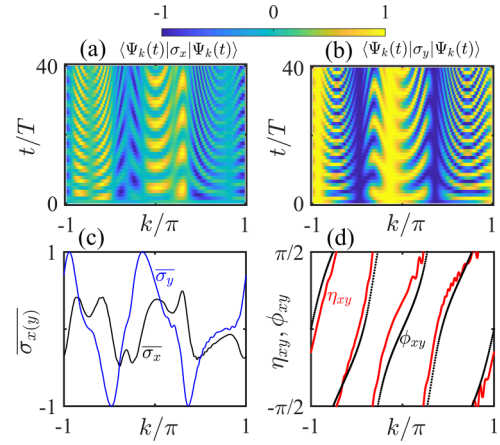


FIG. 5. Extracting conventional winding number via dynamic winding number. (a) and (b) respectively show the time evolution of the stroboscopic spin textures $\langle\psi(k,t)|\sigma_x|\psi(k,t)\rangle$ and $\langle\psi(k,t)|\sigma_y|\psi(k,t)\rangle$. (c) Long-time average of stroboscopic spin textures $\overline{\sigma_x}$ (black line) and $\overline{\sigma_y}$ (blue line) as a function of $k$, and (d) the equilibrium azimuthal angle $\phi_{xy}$ and dynamical azimuthal angle $\eta_{xy}$ as a function of $k$. The other parameters are chosen as $t_1 = 0.3$, $t_2 = 1$, $\xi = 1$, and drive frequency $\omega = 1.2$.

two approaches to restore the original chiral symmetry of the effective Hamiltonian $H_s^{\text{eff}}(k)$. The first approach is to increase the driving frequency $\omega$ in order to reduce the coupling between Floquet bands, which is only applicable in the high-frequency regime. Without limitations on the driving frequency $\omega$, another approach requires that the periodic driving function $F(t)$ be an even function of time $t$, which satisfies $F(t) = F(-t)$. If we consider the initial phase $\theta = \frac{(2n-1)\pi}{2}$, $n = 1, 2, 3, \ldots$, we have $\sigma_z H(k,t)\sigma_z^{-1} = -H(k,t) = -H(k,-t)$, where $\sigma_z$ denotes the chiral symmetry of the original Hamiltonian. We have $\sigma_z U_s(k,T)\sigma_z^{-1} = -U_s(k,T) = U_s(k,-T)$, which yields $\sigma_z H_s^{\text{eff}}(k)\sigma_z^{-1} = -H_s^{\text{eff}}(k)$. Thus, the effective Hamiltonian $H_s^{\text{eff}}(k)$ also has the chiral symmetry $\sigma_z$. Then, the topology can also be detected via the measurement of the DWN, which satisfies

$$w_d = \frac{1}{2\pi}\oint_S \partial_k \eta_{ij}(k)dk, \tag{25}$$

with the dynamical azimuthal angle $\eta_{ij}(k) = \arctan(\overline{\sigma_i}/\overline{\sigma_j})$ based on the stroboscopic long-time-averaged spin textures,

$$\overline{\sigma_i} = \lim_{N\to\infty}\frac{1}{N}\sum_{n=0}^{N}\langle\Psi_k(nT)|\sigma_i|\Psi_k(nT)\rangle. \tag{26}$$

Note that the redefinition of DWN in the low-frequency regime is also applicable to the high-frequency regime. However, in the high-frequency regime one does not have to carry out stroboscopic measurements and properly choose the initial phase. That is why we separately discuss the regimes of low and high frequencies.

As an example, we set the initial phase $\theta = \pi/2$. Based on the time-dependent Hamiltonian (20), we can obtain the stroboscopic spin textures $\langle\Psi_k(nT)|\sigma_{x(y)}|\Psi_k(nT)\rangle$, as shown in Figs. 4(a) and 4(b). The stroboscopic spin textures $\langle\Psi_k(nT)|\sigma_{x(y)}|\Psi_k(nT)\rangle$ oscillate with a momentum-dependent period, and their long-time averages $\overline{\sigma_{x(y)}}$ depending on quasimomentum $k$, see the black and blue lines in Fig. 4(c). Using $\overline{\sigma_x}$ and $\overline{\sigma_y}$, one can calculate the dynamical azimuthal angle $\eta_{xy}$ as a function of $k$, see the red lines in Fig. 4(d). For comparison, we also plot the equilibrium azimuthal angle $\phi_{xy}$ as a function of $k$, see the black lines in Fig. 4(d). Combining with the definitions of $w_\pm$ and $w_d$ in Eqs. (9) and (25), we find that the DWN is equal to 1, which is the same as the CWN $w_\pm$. Then the Zak phase $\Gamma$ can also be calculated using Eq. (13). We find that the Zak phase is equal to $\pi$, which is closely related to the CWN and DWN by $\Gamma/\pi = w_\pm = w_d$. This means that the CWN and Zak phase can also be obtained by measuring $w_d$ in the low-frequency regime with a driving amplitude $\xi = 4$.

Normally, periodic driving can bring several novel topological properties that are usually absent in their static analogs. Unlike previous findings, our system has discovered that periodic driving with low frequency and amplitude can induce another topological property, namely a larger winding number. Interestingly, the larger winding number can also be accurately extracted by DWN. We consider the driving amplitude $\xi = 1$, and the other parameters are the same as those in Fig. 4. Combining the definitions of CWN in Eq. (9), we give the equilibrium azimuthal angle $\phi_{xy}$ as a function of $k$, see the black lines in Fig. 5(d), and then obtain the CWN $w_\pm = 2$. In Figs. 5(a)–5(c), we give the stroboscopic spin textures $\langle\Psi_k(nT)|\sigma_{x(y)}|\Psi_k(nT)\rangle$ and their long-time averages depending on quasimomentum $k$, respectively. Using $\overline{\sigma_x}$ and $\overline{\sigma_y}$, one can calculate the dynamical azimuthal angle $\eta_{xy}$ as a function of $k$, see the red lines in Fig. 5(d). Obviously, combined with the definitions of $w_d$ in Eq. (25), the DWN is equal to 2, which also is the same as the CWN. However, according to the Eq. (13), the Zak phase is equal to 0. This means that the Zak phase is not related to the CWN and DWN, and the DWN can only accurately extract CWN in low-frequency regime with a low driving amplitude $\xi = 1$. Naturally, an open question

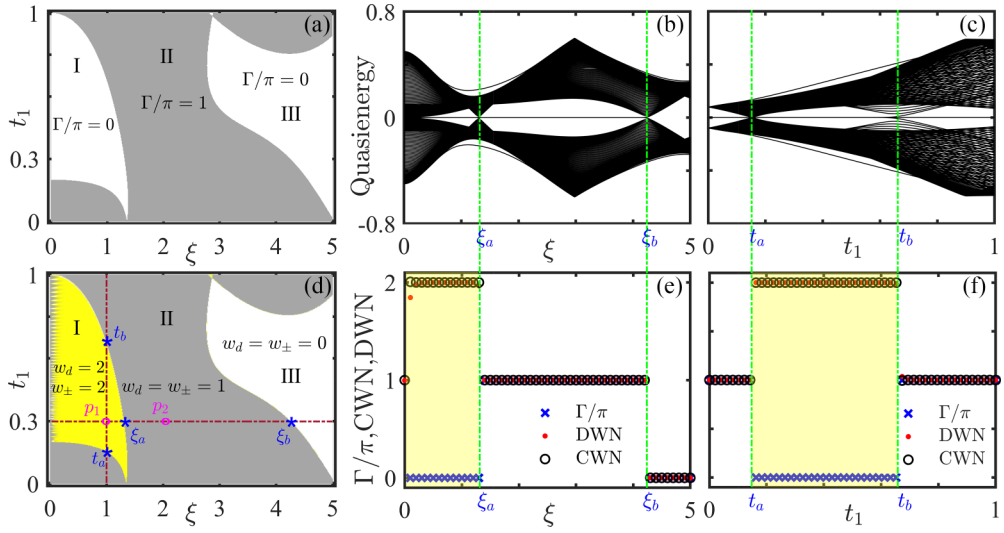


FIG. 6. (a) and (d) show the topological phase diagrams in the parameter plane $(\xi, t_1)$ through the definitions of Zak phase and DWN, respectively. Varying $\xi$ and $t_1$ along the red dashed line in (d), (b), and (c) show the quasienergy spectra under open boundary condition. (e) and (f) respectively correspond to the topological invariant Zak phase $\Gamma/\pi$, CWN and DWN as functions of driving amplitude $\xi$ and coupling strength $t_1$. The other parameters are chosen as $t_2 = 1$ and $\omega = 1.2$.

arises: Which one, the Zak phase or CWN, can accurately characterize the topological properties of the entire parameter space in the low-frequency regime? If the Zak phase can accurately characterize the topological properties of the entire parameter space, then DWN will not be able to accurately measure the topological properties of certain regions of the system. On the contrary, if CWN can accurately depict the topological characteristics of the entire parameter space, this means that the topological invariant extracted by DWN is reliable across the entire parameter space.

To clarify the differences between the Zak phase, CWN, and DWN to represent the topological properties of the system, we present the topological phase diagrams in the parameter plane $(\xi, t_1)$ based on the definitions of the Zak phase, CWN, and DWN, respectively, see Figs. 6(a) and 6(d). For convenience, we will divide the parameter space into three distinct regions, as shown in Figs. 6(a) and 6(d). In region II, it is found that the topological invariant $w_d = w_\pm = \Gamma/\pi = 1$, while in region III, $w_d = w_\pm = \Gamma/\pi = 0$, which correspond to the topological and trivial phases, respectively. However, for region I, the result shows $\Gamma/\pi = 0$, while both CWN and DWN are equal to 2. The Zak phase indicates that the region I is a trivial phase, whereas it is a topologically nontrivial phase with a large topological number using DWN. To understand the underlying causes of this discrepancy, setting the coupling parameter $t_1 = 0.3$, we show the variation of quasienergy and topological invariant with respect to the driving amplitude $\xi$ under open boundary condition [Figs. 6(b) and 6(e)]. Obviously, we can see that the quasienergy spectrum exhibits zero-energy gap closure at $\xi = \xi_a$ and $\xi = \xi_b$ as the driving amplitude $\xi$ increases, where the zero-energy modes exist within the parameter range $\xi \in (0, \xi_b)$. Combined with the topological invariants as a function of the driving amplitude $\xi$ shown in Fig. 6(e), it is evident that the Zak phase cannot accurately characterize the presence of zero-energy modes in the low-frequency regime. When $\xi$ is less than $\xi_a$, the Zak phase $\Gamma/\pi = 0$, while both CWN and DWN are equal to 2. Furthermore, setting the driving amplitude $\xi = 1$, we investigated the variation of quasienergy and topological invariant with respect to the coupling strength $t_1$ under open boundary condition [Figs. 6(c) and 6(f)]. Obviously, we also can see that the quasienergy spectrum exhibits zero-energy gap closure at $t_1 = t_a$ and $t_1 = t_b$ as the coupling parameter $t_1$ increases, where the zero-energy modes always exist. However, when $t_1$ is greater than $t_a$ but less than $t_b$, the Zak phase $\Gamma/\pi = 0$, while both the CWN and DWN are equal to 2. The above results indicate that, compared to the Zak phase, CWN not only is better suited for characterizing the topological properties of the system in the low-frequency regime, but also can be completely detected by measuring the DWN.

### C. Bulk-edge correspondence

Bulk-edge correspondence establishes the exact correspondence between the bulk topological invariant under periodic boundary condition and topological edge states under open boundary condition. In the one-dimensional static system, the emergence of a large topological number typically requires long-range couplings between lattice points. A larger topological number often corresponds to a larger number of topological edge states. Interestingly, unlike static system with long-range couplings, our periodic driving system in the low-frequency regime can also lead to the occurrence of large winding numbers ($w_d = w_\pm = 2$), see the yellow area in Fig. 6(d). To clarify the Bulk-edge correspondence for appearing a large winding number, we give the quasienergy and corresponding Floquet edge states (FESs) for different topological phases in Figs. 7(a) and 7(b), corresponding to the parameter points $p_1$ ($w_d = 2$) and $p_2$ ($w_d = 1$) in Fig. 6(d). For the topological phase with DWN $w_d = 2$, it can be observed that there are four degenerate zero-energy modes within the zero-energy gap, which correspond to four topologically protected FESs [see Fig. 7(a)]. For the topological phase with DWN $w_d = 1$, it can be observed that there are

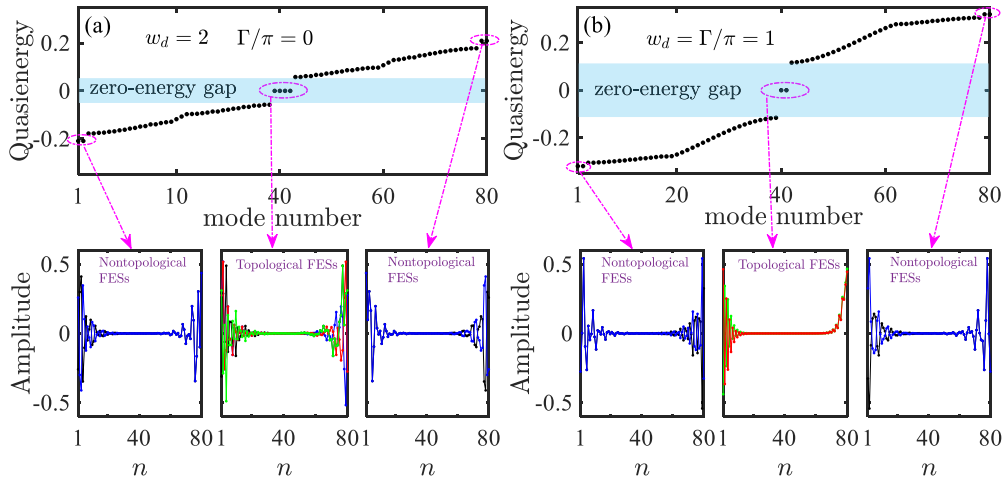


FIG. 7. Quasienergy and Floquet edge states (FESs) with different topological nontrivial phase (a) $w_d = 2$ and (b) $w_d = 1$, respectively corresponding to the parameter points $p_1$ and $p_2$ in Fig. 6(d). The other parameters are chosen as $t_2 = 1$ and $\omega = 1.2$.

two degenerate zero-energy modes within the zero-energy gap, which correspond to two topologically protected FESs [see Fig. 7(b)]. The above results demonstrate that the topological invariant described by DWN still satisfies the principle of bulk-edge correspondence, and then DWN can accurately predict the number of topologically protected FESs.

Furthermore, similar to our previous paper [37], periodic driving can also lead to the generation of nontopological FESs. This is attributed to the creation of virtual defects at the boundary.

## IV. CONCLUSIONS

We presented a unified approach of DWN to characterize the one-dimensional Floquet topological phase with arbitrarily driving frequency. Given a time-averaged spin texture or a stroboscopic time-averaged spin texture in the parameter space, a DWN is given by a loop integral of the dynamical azimuthal angle gradient. In the high-frequency regime, the definition of DWN is based on time-averaged spin textures, which is robust against various initial states and phases. The CWN and Zak phase in the high-frequency regime can be directly given by the corresponding DWN, satisfying the relation $\Gamma = \mathrm{mod}\,(w_d\pi, 2\pi) = \mathrm{mod}\,(w_\pm\pi, 2\pi)$. In the low-frequency regime, the definition of DWN is based on stroboscopic time-averaged spin textures, which also is robust against various initial states, but requires the periodic driving function $F(t)$ to be an even function of time $t$, $F(t) = F(-t)$. Surprisingly, the Zak phase cannot faithfully characterize the topological properties, and the DWN can only accurately extract the CWN in the low-frequency regime with a low driving amplitude, satisfying the relation $w_d = w_\pm$.

According to the bulk-edge correspondence, the DWN can accurately predict the number of topologically protecting Floquet edge states with arbitrarily driving frequency. Compared with previous methods in Refs. [17,49], our schemes clarify the necessity of implementing stroboscopic measurements in Floquet topological insulators and provide a universal definition of DWN in the regimes of arbitrary driving frequency, which does not request any prior knowledge of topology before and after a quench, and also is robust against various initial states.

## ACKNOWLEDGMENTS

This work is supported by the National Natural Science Foundation of China under Grants No.12205385 and No.12175315, the Hunan Provincial Natural Science Foundation under Grant No. 2021JJ41062, the Scientific Research Fund of Hunan Provincial Education Department under Grant No. 23B0264. and the Talent Project of Central South University of Forestry and Technology under Grant No. 2021YJ025. Y.K. is supported by the National Natural Science Foundation of China (Grant No. 12275365) and the Natural Science Foundation of Guangdong (Grant No. 2023A1515012099).

[1] W. Zheng and H. Zhai, Floquet topological states in shaking optical lattices, Phys. Rev. A **89**, 061603(R) (2014).

[2] M. Lababidi, I. I. Satija, and E. Zhao, Counter-propagating edge modes and topological phases of a kicked quantum Hall system, Phys. Rev. Lett. **112**, 026805 (2014).

[3] G. Usaj, P. M. Perez-Piskunow, L. E. F. Foa Torres, and C. A. Balseiro, Irradiated graphene as a tunable Floquet topological insulator, Phys. Rev. B **90**, 115423 (2014).

[4] T. S. Xiong, J. B. Gong, and J. H. An, Towards large-Chern-number topological phases by periodic quenching, Phys. Rev. B **93**, 184306 (2016).

[5] R. Roy and F. Harper, Periodic table for Floquet topological insulators, Phys. Rev. B **96**, 155118 (2017).

[6] M. Rodriguez-Vega and B. Seradjeh, Universal fluctuations of Floquet topological invariants at low frequencies, Phys. Rev. Lett. **121**, 036402 (2018).

[7] M. Rodriguez-Vega, A. Kumar, and B. Seradjeh, Higher-order Floquet topological phases with corner and bulk bound states, Phys. Rev. B **100**, 085138 (2019).

[8] R. W. Bomantara, L. W. Zhou, J. X. Pan, and J. B. Gong, Coupled-wire construction of static and Floquet second-order topological insulators, Phys. Rev. B **99**, 045441 (2019).

[9] Y. Peng and G. Refael, Floquet second-order topological insulators from nonsymmorphic space-time symmetries, Phys. Rev. Lett. **123**, 016806 (2019).

[10] R. Seshadri, A. Dutta, and D. Sen, Generating a second-order topological insulator with multiple corner states by periodic driving, Phys. Rev. B **100**, 115403 (2019).

[11] H. Liu, T. S. Xiong, W. Zhang, and J. H. An, Floquet engineering of exotic topological phases in systems of cold atoms, Phys. Rev. A **100**, 023622 (2019).

[12] K. Yang, L. W. Zhou, W. C. Ma, X. Kong, P. F. Wang, X. Qin, X. Rong, Y. Wang, F. Z. Shi, J. B. Gong, and J. F. Du, Floquet dynamical quantum phase transitions, Phys. Rev. B **100**, 085308 (2019).

[13] M. Umer, R. W. Bomantara, and J. B. Gong, Counterpropagating edge states in Floquet topological insulating phases, Phys. Rev. B **101**, 235438 (2020).

[14] M. S. Rudner, N. H. Lindner, E. Berg, and M. Levin, Anomalous edge states and the bulk-edge correspondence for periodically driven two-dimensional systems, Phys. Rev. X **3**, 031005 (2013).

[15] F. Nathan and M. S. Rudner, Topological singularities and the general classification of Floquet–Bloch systems, New J. Phys. **17**, 125014 (2015).

[16] M. S. Rudner and N. H. Lindner, Band structure engineering and non-equilibrium dynamics in Floquet topological insulators, Nat. Rev. Phys. **2**, 229 (2020).

[17] L. Zhang, L. Zhang, and X. J. Liu, Unified theory to characterize Floquet topological phases by quench dynamics, Phys. Rev. Lett. **125**, 183001 (2020).

[18] Y. Jia and Z. Li, High winding number of topological phase in periodic quantum walks, Phys. Lett. A **399**, 127303 (2021).

[19] K. Y. Shi, R. Q. Chen, S. N. Zhang, and W. Zhang, Topological invariants of Floquet topological phases under periodical driving, Phys. Rev. A **106**, 053301 (2022).

[20] K. Yang, S. Y. Xu, L. W. Zhou, Z. Y. Zhao, T. Y. Xie, Z. Ding, W. C. Ma, J. B. Gong, F. Z. Shi, and J. F. Du, Observation of Floquet topological phases with large Chern numbers, Phys. Rev. B **106**, 184106 (2022).

[21] Y. G. Peng, C. Z. Qin, D. G. Zhao, Y. X. Shen, X. Y. Xu, M. Bao, H. Jia, and X. F. Zhu, Experimental demonstration of anomalous Floquet topological insulator for sound, Nat. Commun. **7**, 13368 (2016).

[22] N. Fläschner, B. S. Rem, M. Tarnowski, D. Vogel, D. S. Lühmann, K. Sengstock, and C. Weitenberg, Experimental reconstruction of the Berry curvature in a Floquet Bloch band, Science **352**, 1091 (2016).

[23] S. Mukherjee, A. Spracklen, M. Valiente, E. Andersson, P. Öhberg, N. Goldman, and R. R. Thomson, Experimental observation of anomalous topological edge modes in a slowly driven photonic lattice, Nat. Commun. **8**, 13918 (2017).

[24] L. J. Maczewsky, J. M. Zeuner, S. Nolte, and A. Szameit, Observation of photonic anomalous Floquet topological insulators, Nat. Commun. **8**, 13756 (2017).

[25] C. Chen, X. Ding, J. Qin, J. Z. Wu, Y. He, C. Y. Lu, L. Li, X. J. Liu, B. C. Sanders, and J. W. Pan, Topological spin texture of chiral edge states in photonic two-dimensional quantum walks, Phys. Rev. Lett. **129**, 046401 (2022).

[26] W. Hu, J. C. Pillay, K. Wu, M. Pasek, P. P. Shum, and Y. D. Chong, Measurement of a topological edge invariant in a microwave network, Phys. Rev. X **5**, 011012 (2015).

[27] K. Wintersperger, C. Braun, F. N. Ünal, A. Eckardt, M. D. Liberto, N. Goldman, I. Bloch, and M. Aidelsburger, Realization of an anomalous Floquet topological system with ultracold atoms, Nat. Phys. **16**, 1058 (2020).

[28] X. T. Lu, T. Wang, T. Li, C. H. Zhou, M. J. Yin, Y. B. Wang, X. F. Zhang, and H. Chang, Doubly modulated optical lattice clock: Interference and topology, Phys. Rev. Lett. **127**, 033601 (2021).

[29] J. Y. Zhang, C. R. Yi, L. Zhang, R. H. Jiao, K. Y. Shi, H. Yuan, W. Zhang, X. J. Liu, S. Chen, and J. W. Pan, Tuning anomalous Floquet topological bands with ultracold atoms, Phys. Rev. Lett. **130**, 043201 (2023).

[30] X. L. Qi and S. C. Zhang, Topological insulators and superconductors, Rev. Mod. Phys. **83**, 1057 (2011).

[31] B. A. Bernevig and T. L. Hughes, *Topological Insulators and Topological Superconductors* (Princeton University Press, Princeton, NJ, 2013).

[32] Y. Ando, Topological insulator materials, J. Phys. Soc. Jpn. **82**, 102001 (2013).

[33] C. K. Chiu, J. C. Y. Teo, A. P. Schnyder, and S. Ryu, Classification of topological quantum matter with symmetries, Rev. Mod. Phys. **88**, 035005 (2016).

[34] B. Q. Lv, Z. L. Feng, Q. N. Xu, X. Gao, J. Z. Ma, L. Y. Kong, P. Richard, Y. B. Huang, V. N. Strocov, C. Fang *et al.*, Observation of three-component fermions in the topological semimetal molybdenum phosphide, Nature (London) **546**, 627 (2017).

[35] T. Ozawa, H. M Price, A. Amo, N. Goldman, M. Hafezi, L. Lu, M. C. Rechtsman, D. Schuster, J. Simon, O. Zilberberg, and I. Carusotto, Topological photonics, Rev. Mod. Phys. **91**, 015006 (2019).

[36] V. Dal Lago, M. Atala, and L. E. F. Foa Torres, Floquet topological transitions in a driven one-dimensional topological insulator, Phys. Rev. A **92**, 023624 (2015).

[37] B. Zhu, H. H. Zhong, Y. G. Ke, X. Z. Qin, A. A. Sukhorukov, Y. S. Kivshar, and C. Lee, Topological Floquet edge states in periodically curved waveguides, Phys. Rev. A **98**, 013855 (2018).

[38] J. M. Zeuner, M. C. Rechtsman, Y. Plotnik, Y. Lumer, S. Nolte, M. S. Rudner, M. Segev, and A. Szameit, Observation of a topological transition in the bulk of a non-Hermitian system, Phys. Rev. Lett. **115**, 040402 (2015).

[39] S. Longhi, Probing one-dimensional topological phases in waveguide lattices with broken chiral symmetry, Opt. Lett. **43**, 4639 (2018).

[40] F. Cardano, A. D' Errico, A. Dauphin, M. Maffei, B. Piccirillo, C. de Lisio, G. De Filippis, V. Cataudella, E. Santamato, L. Marrucci *et al.*, Detection of Zak phases and topological invariants in a chiral quantum walk of twisted photons, Nat. Commun. **8**, 15516 (2017).

[41] W. Sun, C. R. Yi, B. Z. Wang, W. W. Zhang, B. C. Sanders, X. T. Xu, Z. Y. Wang, J. Schmiedmayer, Y. Deng, X. J.

Liu *et al.*, Uncover topology by quantum quench dynamics, Phys. Rev. Lett. **121**, 250403 (2018).

[42] L. Zhang, L. Zhang, S. Niu, and X. J. Liu, Dynamical classification of topological quantum phases, Sci. Bull. **63**, 1385 (2018).

[43] L. Zhang, L. Zhang, and X. J. Liu, Dynamical detection of topological charges, Phys. Rev. A **99**, 053606 (2019).

[44] L. Li, W. Zhu, and J. Gong, Direct dynamical characterization of higher-order topological phases with nested band inversion surfaces, Sci. Bull. **66**, 1502 (2021).

[45] W. Jia, X. C. Zhou, L. Zhang, L. Zhang, and X. J. Liu, Unified characterization for higher-order topological phase transitions, Phys. Rev. Res. **5**, L022032 (2023).

[46] C. Wang, P. Zhang, X. Chen, J. Yu, and H. Zhai, Scheme to measure the topological number of a Chern insulator from quench dynamics, Phys. Rev. Lett. **118**, 185701 (2017).

[47] M. Tarnowski, F. N. Ünal, N. Fläschner, B. S. Rem, A. Eckardt, K. Sengstock, and C. Weitenberg, Measuring topology from dynamics by obtaining the Chern number from a linking number, Nat. Commun. **10**, 1728 (2019).

[48] B. Zhu, Y. G. Ke, H. H. Zhong, and C. Lee, Dynamic winding number for exploring band topology, Phys. Rev. Res. **2**, 023043 (2020).

[49] L. W. Zhou, Dynamical characterization of non-Hermitian Floquet topological phases in one dimension, Phys. Rev. B **100**, 184314 (2019).

[50] G. Platero and R. Aguado, Photon-assisted transport in semiconductor nanostructures, Phys. Rep. **395**, 1 (2004).

[51] A. Gómez-León and G. Platero, Floquet-Bloch theory and topology in periodically driven lattices, Phys. Rev. Lett. **110**, 200403 (2013).

[52] J. Zak, Berry's phase for energy bands in solids, Phys. Rev. Lett. **62**, 2747 (1989).

[53] C. Yin, H. Jiang, L. Li, R. Lü, and S. Chen, Geometrical meaning of winding number and its characterization of topological phases in one-dimensional chiral non-Hermitian systems, Phys. Rev. A **97**, 052115 (2018).